Applied Physics Letters

RESEARCH ARTICLE | DECEMBER 18 2023

Color-selective optical edge detection enabled by thermally stimulated cholesteric liquid crystals

Quan-Ming Chen ; Hua-Cai Wang ; Guang-Yao Wang ; Chun-Ting Xu ; Qing-Gui Tan; Wei Duan ; Yan-Qing Lu ; Wei Hu

Appl. Phys. Lett. 123, 251101 (2023)
https://doi.org/10.1063/5.0170808

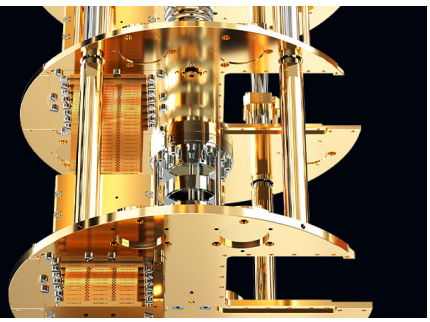

Applied Physics Letters ARTICLE pubs.aip.org/aip/apl

Color-selective optical edge detection enabled by thermally stimulated cholesteric liquid crystals

Cite as: Appl. Phys. Lett. **123**, 251101 (2023); doi: 10.1063/5.0170808
Submitted: 4 August 2023 · Accepted: 7 November 2023 ·
Published Online: 18 December 2023

View Online Export Citation CrossMark

Quan-Ming Chen,[1] Hua-Cai Wang,[1] Guang-Yao Wang,[1] Chun-Ting Xu,[1] Qing-Gui Tan,[2] Wei Duan,[3,a)] Yan-Qing Lu,[1] and Wei Hu[1,a)]

AFFILIATIONS

[1]National Laboratory of Solid State Microstructures, College of Engineering and Applied Sciences, Nanjing University, Nanjing 210023, China
[2]China Academy of Space Technology, National Key Laboratory of Science and Technology on Space Microwave, Xi'an, China
[3]Beihang University, School of Instrumentation and Optoelectronic Engineering, Beijing, China

[a)]**Authors to whom correspondence should be addressed:** wduan@buaa.edu.cn and huwei@nju.edu.cn

ABSTRACT

Optical edge detection can significantly compress the data volume and is highly pursued in imaging processing. The commonly used methods extract the optical edge information but lose the capability to distinguish colors, which is another key information for imaging. Here, a design for color-selective optical edge detection is proposed and demonstrated with a cholesteric liquid crystal *q*-plate. The corresponding optical edge detection exhibits a narrow reflection band characteristic due to the one-dimensional photonic crystal configuration of the cholesteric liquid crystal. The monochromatic band is thermally and reversibly tuned ~300 nm within 5.3 °C. Color-selective optical edge detection is verified by a series of chromatic images. This work introduces a thermally responsive liquid crystal device to release the color dimension of optical edge detection, which may upgrade existing imaging processing techniques.

Instant imaging processing is highly demanded in self-driving vehicles, drone swarm attacks, and automatic optical inspections in smart factories. Data compression is, thus, a key requirement for saving computing power and reducing the time delay.[1,2] Since the edge preserves the most useful geometrical features of various objects, edge detection has been proven to be efficient in alleviating the information load. Various physical effects, such as the photonic spin Hall effect,[3] Goos–Hänchen shift,[4] and Brewster's angle,[5] have been used to directly extract edge information by spatial differentiation via light-matter interactions. Different materials, including photonic crystal slabs[6] and metasurfaces,[7] have been adopted. Optical edge detection provides a time/energy-saving tool for imaging processing. However, the absence of other information dimensions affects the accuracy of target recognition, which could result in accidents, mission failures, or production failures. Color is an important dimension of imaging that usually contains both configuration and composition information. Thereby, color distinguishable optical edge detection is highly pursued. For ordinary optical differentiators, their working wavelengths are fixed once fabricated. A device that can extract edge information with wavelength selectivity, thus, becomes a necessary requirement.

Broadband edge detection across the visible range has been realized by a metasurface with a gradient Pancharatnam–Berry (PB) phase made of form-birefringent nanostructured glass slabs[8] as well as a spiral phase plate made of titanium dioxide-based metasurface.[9] However, different monochromatic components of the object cannot be individually separated. Liquid crystal (LC)-based planar optics is a perfect candidate for PB phase modulation.[10,11] The external field responsiveness further enables the elements to tune the working band.[12] For cholesteric LC (CLC), elongated molecules assemble into a periodic helical superstructure, thus forming a one-dimensional photonic crystal.[13] Light with wavelengths falling within the Bragg band and the same handedness as the helicity of CLC is totally reflected, and the residual energy transmits directly.[14] By presetting the local initial orientations, the spatial Bragg–Berry reflection can be freely programmed.[15,16] Recently, a CLC-based reflective edge detection device was presented.[17] Inspired by external stimuli, the helical pitch can be continuously varied. This unique characteristic has inspired tremendous active light modulations, such as beam steering[18] and bandwidth scalable holographic displays.[19] Exploiting a dynamic CLC-based solution for color-selective optical edge detection is, thus, meaningful and will promote the development of active optical analog computing.

In this work, we present color-selective optical edge detection with a thermally responsive CLC q-plate. Along with the continuous helical pitch variation of CLC, a reversible reflection band shift ~300 nm is demonstrated within the temperature range of 5.3 °C. Thanks to the wavelength selectivity, the edge information of chromatic images is selectively extracted by colors. The uniformity is well maintained during the structural evolution, leading to high-quality color-selective optical edge detection. This work opens a door for active optical edge detection in wide fields involving imaging processing.

The design of the CLC-based color-selective optical edge detector is schematically illustrated in Fig. 1. The helical pitch p, depicting the distance that LC directors continuously rotate 2π along the helical axis, is expressed as[20]

$$p = \frac{1}{c \times \mathrm{HTP}}, \tag{1}$$

where c and HTP denote the weight concentration and helical twisting power of the chiral dopant, respectively. The central wavelength (λ_c) of the Bragg reflection band satisfies[20]

$$\begin{aligned} \lambda_c &= \bar{n} \cdot p \\ \bar{n} &= \frac{n_e + n_o}{2}, \end{aligned} \tag{2}$$

where $\bar{n}$, n_o, and n_e are the average, ordinary, and extraordinary indices, respectively. A spiral distribution of azimuthal orientation $\alpha = 0.5\arctan(v/u)$ is encoded to guide the initial orientations of the CLC, thus forming a reflective q-plate with $q = 0.5$, as shown in Fig. 1(a). Light selectively reflected by such a structure carries a spiral phase of 2α. When adopted with a thermally sensitive chiral dopant, the HTP decreases with decreasing temperature. Therefore, p increases and λ_c redshifts [Fig. 1(b)].[21] When the sample is placed at the central Fourier plane (u, v) of a 4f imaging system, according to the Fourier convolution theorem, the output light field $E_{out}(x, y)$ can be expressed as

$$E_{out}(x, y) = E_{in}(x, y) \otimes t(x, y), \tag{3}$$

where $E_{in}(x, y)$ is the incident electric field of the object in Cartesian coordinates (x, y), $\otimes$ denotes the convolution, and $t(x, y)$ is the Fourier transform (or convolution kernel) of the spiral phase. $E_{out}(x, y)$ satisfies[22]

$$E_{out}(x, y) \propto g_a(x, y) e^{i\varphi_{in}(x,y)} e^{i\delta_a(x,y)} + i g_p E_{in}(x, y) e^{i\delta_p(x,y)}, \tag{4}$$

where $\varphi_{in}(x, y)$ is the phase of the object. g_a and g_p are the amplitude and phase gradients of $E_{in}(x, y)$, respectively. δ_a and δ_p are the corresponding polar angles. For the plane wave ($g_p = 0$) illuminated or reflected by the object, the q-plate encodes a spiral phase $e^{i2\alpha}$ to the light. Therefore, when $g_a = 0$, $E_{out}(x, y)$ is totally suppressed, and light only exists where $g_a \neq 0$. This is the principle for optical edge detection. Combined with the wavelength selectivity of the thermally tuned CLC, color-selective optical edge detection can, thus, be realized. Here, the CLC q-plate is a pure phase modulator that utilizes all the light of same circular polarization for optical edge detection, which is totally different from the conventional high frequency pass (HFP) filter. Thereby, the reconfigurable CLC q-plate works as an integrated optical processor with a distinct physical mechanism compared to the HFP to release the color dimension of optical edge detection. The cartoon in Fig. 1(c) vividly presents the extraction of monochromatic edges from a chromatic image during thermal cycling.

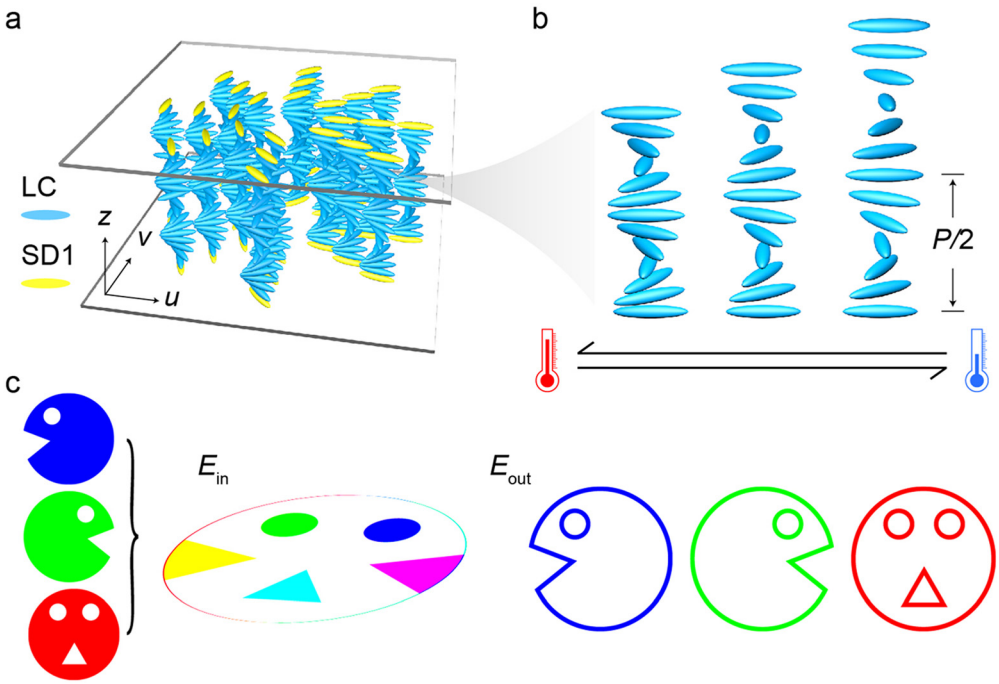

FIG. 1. (a) The configuration of a CLC q-plate. (b) Thermally induced p variation. (c) Schematic diagram for color-selective optical edge detection.

The thermally tuned CLC was mixed with nematic host E7 (NCLCP, China) and left-handed chiral dopant S811 (NCLCP, China), whose helical twisting power is 8.3 μm^{-1} at 30 °C. An optimized c of 32 wt. % is adopted to realize a broad tunable range of the color. The color selectivity is verified with a unidirectionally and parallelly aligned cell (cell gap 10 μm). As shown in Fig. 2(a), λ_c redshifts from 460 to 750 nm during the cooling process from 35.2 °C to 29.9 °C at a slow rate of −0.3 °C/min (Linkam LTS120, UK). The nematic range of the CLC mixture is tested (Fig. S1). It covers the operating temperature range (29.9–35.2 °C) of the CLC q-plate in our work, and no precipitation of S811 is observed under POM at this condition. The thermal tuning of λc mainly results from two facts: the temperature dependent solubility of S811[23] and the temperature dependent refractive indices of E7.[24] λ_c blueshifts to the initial state after heating back. The total tunable band covers most of the visible range (440–780 nm). The CLC q-plate is fabricated using a digital-micromirror-device based photopatterning system[25] to record the designed alignment to photoalignment agent azo-dye SD1 layers[26] (NCLCP, China). Uniform sharp reflective colors are observed under a polarized optical microscope (POM) (Nikon 50i, Japan), as revealed in Fig. 2(b). Along with the varying temperatures, donut-like optical vortices of different colors consistent with the simulation are selectively reflected [Fig. 2(c)]. The astigmatic transformation is adopted to detect the topological charge of the generated optical vortices, which is −1 according to the number of dark stripes and their tilt direction.

The aforementioned facts indicate the feasibility of color-selective optical edge detection based on a CLC q-plate. Herein, a reflective 4f imaging system is prepared for characterization. As shown in Fig. 3(a),

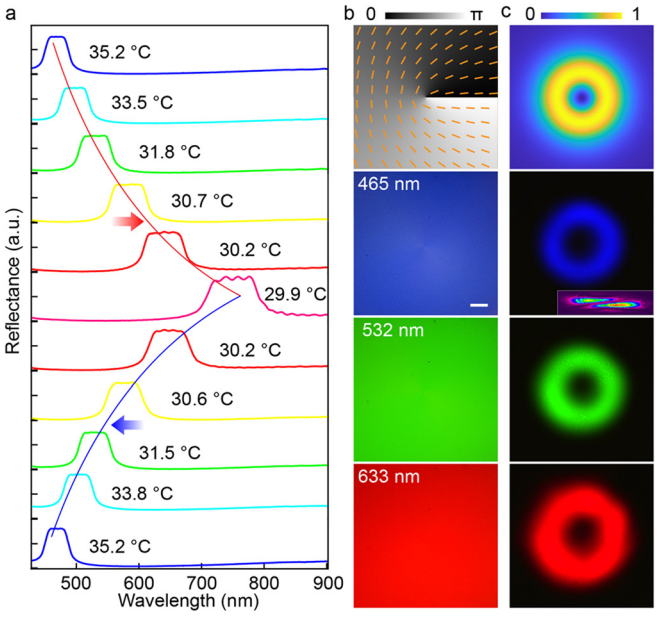

FIG. 2. Thermally tunable CLC q-plate. (a) The shift of reflection bands dependent on temperature variation. (b) α of the CLC q-plate with $q = 0.5$ and corresponding POM images recorded when $\lambda_c = 465$, 532, and 633 nm. (c) Simulated intensity distribution and experimentally obtained optical vortices with the CLC q-plate. The inset under the blue optical vortex reveals the topological charge characterized by the astigmatic transformation. The scale bar indicates 200 μm for all micrographs.

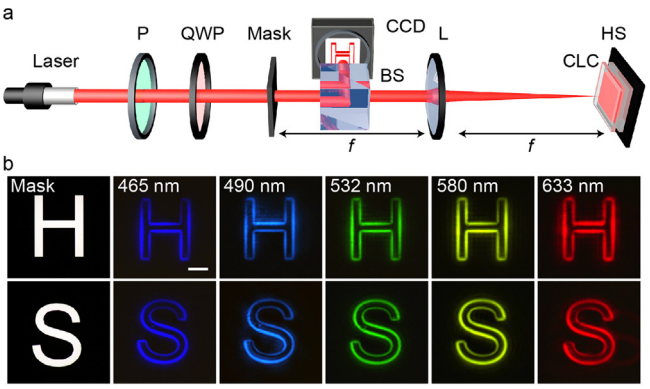

FIG. 3. Optical edge detection. (a) The experimental setup. P, QWP, BS, L, and HS are the polarizer, broadband quarter waveplate, unpolarized beam splitter, lens and hot stage, respectively. (b) Edge detection results of capital letters H and S during the varying of temperature. The scale bar indicates 200 μm.

a supercontinuum laser (SuperK EVO, NKT Photonics, Denmark) is used as a broadband tunable light source, and different monochromatic lasers with bandwidth < 5 nm are filtered by an acousto-optic filter (SuperK SELECT, NKT, Denmark). The power for filtered and collimated single wavelength laser is in microwatts scale. A polarizer and a broadband quarter waveplate are adopted to generate left-handed circular polarization matching with the helicity of CLC. The beam passes through hollow masks of capital letters "H" and "S" and works as the object for edge detection. The CLC q-plate is placed at the rear Fourier plane of the lens. A charge-coupled device (CCD) is placed at the front Fourier plane of the same lens through an unpolarized beam splitter. With this optical path, broadband tunable optical edge detection based on the CLC q-plate is verified. With varying temperature, only light within the Bragg band is selectively reflected and encoded with a spiral phase $e^{i2\alpha}$ by the sample. Correspondingly, monochromatic edge information of the target is subsequently obtained. Figure 3(b) reveals images at 465, 490, 532, 580, and 633 nm. The thermally tuned pitch covers almost the entire visible range. The edge information of H has been extracted clearly in both lateral and horizontal directions. The case of S further confirms that the edge detection is irrespective of objects' orientations and curvatures. The edge detection resolution is measured as 31.25, 35.08, 35.08, 39.37, and 39.37 μm for 465, 490, 532, 580, and 633 nm, respectively. It can be further improved by optimizing the efficiency of the spiral phase modulation and the numerical aperture of the reflective 4f imaging system. b/w transmission masks are commonly used as the object for similar optical edge detections. However, the edge detection is not restricted to binary images. The optical edge detection for grayscale images (Fig. S3) is also verified. In addition, the optical edge detector also works for the low contrast image (Fig. S4).

The proposed detector is suitable for distinguishing edges of different colors. For proof demonstration, two wavelength channels pass separate 1951 United States Air Force (USAF) resolution test charts [Fig. 4(a)] and are then combined by a beam splitter to form a chromatic object. Notably, the birefringence of E7 exhibits a wavelength dependency;[27] therefore, its influence on the photonic bandgap tailoring should be further taken into consideration in the white light experiments. As shown in Fig. 4(b), different combinations of red

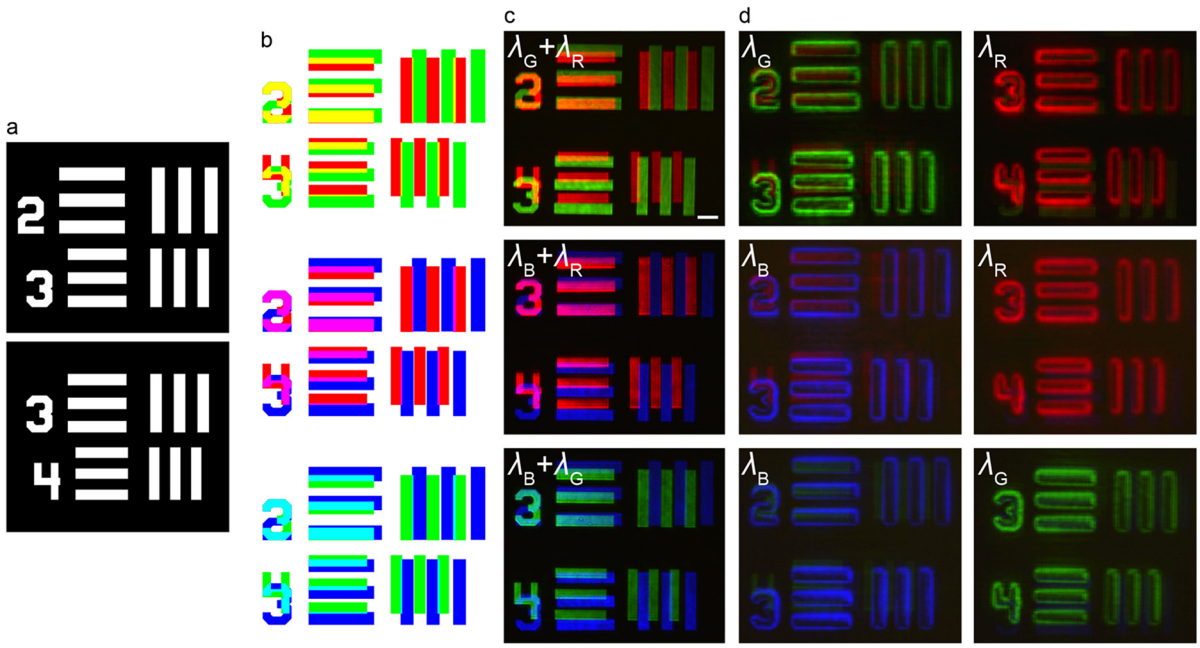

FIG. 4. Color-selective optical edge detection. (a) Two hollow masks. (b) Different color combinations transmitting individual masks. (c) Images of objects with different wavelengths. λ_B, λ_G, and $\lambda_R = 465$, 532, and 633 nm, respectively. (d) Color-selective optical edge detection enabled by a thermal stimulus. The scale bar indicates 400 μm.

($\lambda_R = 633$ nm), green ($\lambda_G = 532$ nm), and blue ($\lambda_B = 465$ nm) lasers pass through individual hollow masks and then illuminate the sample. The reflectivity for the circularly polarized light of the same handedness to CLC is 91.2%, 90.6%, and 89.2% at 465, 532, and 633 nm, respectively (Fig. S5). The generated chromatic images are shown in Fig. 4(c), in which the overlapping and separation of different colors are clearly observed. By tuning the temperature, different colored edges are recorded, as presented in Fig. 4(d). Only the edge information of selected wavelengths is detected, while the weak mismatched components are observed due to mirror reflection from the front substrate of the LC cell. The mirror reflection can be effectively suppressed with antireflective layers. The aforementioned experiments vividly verify the color-selective optical edge detection function of the proposed CLC q-plate.

Compared to previously reported broadband optical edge detectors, the proposed thermally tuned CLC q-plate here supplies real wavelength-selective edge detection across the visible range. It, thus, enables the simultaneous detection of both edge and color information, which may significantly enhance the accuracy of object recognition. Thanks to the intrinsic helical structure of CLC, circular polarization of same handedness is selectively extracted for edge detection, while the opposite component transmits the sample and can be used for direct imaging. Although only three wavelength channels are presented here, at most seven channels can be realized with negligible crosstalk according to the spectra revealed in Fig. 2(a). More channels are expected by introducing LCs with smaller birefringence[13] or blue-phase LCs[28] with narrower reflection bands. The CLC q-plate is feasible for phase gradient objects ($g_a = 0$) as well. Combined with the wavelength selectivity, this device has potentials in biomedical research.[29,30] Thanks to the high efficiency of the spiral phase modulation, the proposed reflective optical edge detector is available in real environment even considering the loss induced by the BS. Here, the thermally tuned CLC q-plate is just presented as a proof-of-principle demonstration for the color-selective optical edge detection. Actually, the stimulus is not restricted to thermal, and other physical field such as photo and electricity as well as fast response materials such as blue-phase LCs can be adopted, enabling more rapid shifting of the band. The wavelength can also be tuned by electricity, which may make the operation of the optical edge detector much faster.[31,32]

In summary, we proposed and demonstrated a color-selective optical edge detector based on a CLC q-plate. Under thermal stimulation, the evolution of the helical structure enables broadband reversible wavelength selectivity. Combining the spiral phase encoding with the wavelength selectivity, high-quality detections of edges in different colors were realized. It makes the synchronous detection of edge and color information possible and may significantly enhance the accuracy of object recognition. This work introduced LC superstructures to active optical edge detection and may upgrade existing imaging processing.

See the supplementary material for the DSC measurement, optical edge detections for grayscale and low contrast objects, and the reflective spectra of the CLC q-plate.

The authors appreciate the support from the National Key Research and Development Program of China (No. 2022YFA1203703), the National Natural Science Foundation of China (NSFC) (Nos. 62035008 and 62005009), the Stable Support Fund of State Administration Science Technology and Industry for National Defense (No. HTKJ2022KL504003), and the Fundamental

Research Funds for the Central Universities (No. 021314380233). The authors gratefully appreciate JCOPTIX for providing optical test equipment.

AUTHOR DECLARATIONS

Conflict of Interest

The authors have no conflicts to disclose.

Author Contributions

Quan-Ming Chen: Data curation (lead); Formal analysis (equal); Methodology (lead); Software (lead); Validation (lead); Visualization (lead); Writing – original draft (lead); Writing – review & editing (equal). **Hua-Cai Wang:** Formal analysis (equal); Methodology (equal); Software (equal); Validation (equal); Visualization (equal). **Guang-Yao Wang:** Formal analysis (equal); Writing – review & editing (equal). **Chun-Ting Xu:** Formal analysis (equal); Writing – review & editing (equal). **Qinggui Tan:** Formal analysis (equal); Resources (equal); Writing – review & editing (equal). **Wei Duan:** Conceptualization (equal); Formal analysis (equal); Methodology (equal); Resources (equal); Writing – review & editing (equal). **Yan-Qing Lu:** Resources (equal); Supervision (equal); Writing – review & editing (equal). **Wei Hu:** Conceptualization (lead); Formal analysis (equal); Funding acquisition (lead); Resources (lead); Supervision (lead); Writing – review & editing (equal).

DATA AVAILABILITY

The data that support the findings of this study are available from the corresponding author upon reasonable request.

REFERENCES

[1]H. J. Caulfield and S. Dolev, Nat. Photonics **4**(5), 261 (2010).
[2]D. R. Solli and B. Jalali, Nat. Photonics **9**(11), 704 (2015).
[3]T. F. Zhu, Y. J. Lou, Y. H. Zhou, J. H. Zhang, J. Y. Huang, Y. Li, H. L. Luo, S. C. Wen, S. Y. Zhu, and Q. H. Gong, Phys. Rev. Appl. **11**(3), 034043 (2019).
[4]D. Y. Xu, S. S. He, J. X. Zhou, S. Z. Chen, S. C. Wen, and H. L. Luo, Appl. Phys. Lett. **116**(21), 211103 (2020).
[5]D. Y. Xu, S. S. He, J. X. Zhou, S. Z. Chen, S. C. Wen, and H. L. Luo, Opt. Lett. **45**(24), 6867 (2020).
[6]C. Guo, M. Xiao, M. Minkov, Y. Shi, and S. H. Fan, Optica **5**(3), 251 (2018).
[7]S. He, R. Wang, and H. Luo, Nanophotonics **11**(6), 1083 (2022).
[8]J. Zhou, H. Qian, C. Chen, J. Zhao, G. Li, Q. Wu, H. Luo, S. Wen, and Z. Liu, Proc. Natl. Acad. Sci. U. S. A. **116**(23), 11137 (2019).
[9]P. Huo, C. Zhang, W. Zhu, M. Liu, S. Zhang, S. Zhang, L. Chen, H. J. Lezec, A. Agrawal, Y. Lu, and X. Ting, Nano Lett. **20**(4), 2791 (2020).
[10]P. Chen, B. Wei, W. Hu, and Y. Lu, Adv. Mater. **32**(27), 1903665 (2020).
[11]J. H. Xiong and S. T. Wu, eLight **1**(1), 3 (2021).
[12]Q. Chen, C. Xu, X. Liang, and W. Hu, Adv. Quantum Technol. **6**(2), 2200153 (2023).
[13]D. K. Yang and S. T. Wu, *Fundamentals of Liquid Crystal Devices* (John Wiley & Sons, 2014).
[14]Q. M. Chen, Z. H. Peng, Y. Li, S. X. Liu, P. C. Zhou, J. Y. Gu, J. G. Lu, L. S. Yao, M. Wang, and Y. K. Su, Opt. Express **27**(9), 12039 (2019).
[15]J. Kobashi, H. Yoshida, and M. Ozaki, Nat. Photonics **10**(6), 389 (2016).
[16]M. Rafayelyan, G. Tkachenko, and E. Brasselet, Phys. Rev. Lett. **116**(25), 253902 (2016).
[17]T. B. Zeng, J. Xie, Y. J. Zhou, F. Fan, and S. C. Wen, Opt. Lett. **48**(3), 795 (2023).
[18]P. Chen, L. L. Ma, W. Hu, Z. X. Shen, H. K. Bisoyi, S. B. Wu, S. J. Ge, Q. Li, and Y. Q. Lu, Nat. Commun. **10**(1), 2518 (2019).
[19]C. T. Xu, D. W. Zhang, R. Yuan, Q. M. Chen, X. Liang, and W. Hu, Laser Photonics Rev. **17**(7), 2201013 (2023).
[20]P.-G. De Gennes and J. Prost, *The Physics of Liquid Crystals* (Oxford University Press, 1993).
[21]P. C. Wu, G. W. Wu, I. V. Timofeev, V. Y. Zyryanov, and W. Lee, Photonics Res. **6**(12), 1094 (2018).
[22]A. Jesacher, S. Fürhapter, S. Bernet, and M. Ritsch-Marte, J. Opt. Soc. Am. A **23**(6), 1400 (2006).
[23]Y. H. Huang, Y. Zhou, C. Doyle, and S. T. Wu, Opt. Express **14**(3), 1236 (2006).
[24]J. Li, C. H. Wen, S. Gauza, R. Lu, and S. T. Wu, J. Disp. Technol. **1**(1), 51 (2005).
[25]H. Wu, W. Hu, H. C. Hu, X. W. Lin, G. Zhu, J. W. Choi, V. Chigrinov, and Y. Q. Lu, Opt. Express **20**(15), 16684 (2012).
[26]V. Chigrinov, S. Pikin, A. Verevochnikov, V. Kozenkov, M. Khazimullin, J. Ho, D. D. Huang, and H.-S. Kwok, Phys. Rev. E **69**(6), 061713 (2004).
[27]S. T. Wu, Phys. Rev. A **33**(2), 1270 (1986).
[28]J. Yan, S. T. Wu, K. L. Cheng, and J. W. Shiu, Appl. Phys. Lett. **102**(8), 081102 (2013).
[29]J. X. Zhou, H. L. Qian, J. X. Zhao, M. Tang, Q. Y. Wu, M. Lei, H. L. Luo, S. C. Wen, S. C. Chen, and Z. W. Liu, Natl. Sci. Rev. **8**(6), nwaa176 (2021).
[30]J. Zhou, Q. Wu, J. Zhao, C. Posner, M. Lei, G. Chen, J. Zhang, and Z. Liu, Phys. Rev. Lett. **129**(2), 020801 (2022).
[31]C. L. Yuan, W. B. Huang, Z. G. Zheng, B. H. Liu, H. K. Bisoyi, Y. N. Li, D. Shen, Y. Q. Lu, and Q. Li, Sci. Adv. **5**(10), eaax9501 (2019).
[32]C. Xu, B. Liu, C. Peng, Q. Chen, P. Chen, P. Sun, Z. Zheng, Y. Lu, and W. Hu, Adv. Opt. Mater. **10**(19), 2201088 (2022).